Pergamon

PII: S0021-8502(96)00054-7

J. Aerosol Sci. Vol. 28, No. 1, pp. 35–52, 1997
Copyright © 1996 Elsevier Science Ltd
Printed in Great Britain. All rights reserved
0021-8502/96 $17.00 + 0.00

MOTION OF DIFFUSIONLESS PARTICLES IN VERTICAL STAGNATION FLOWS—II. DEPOSITION EFFICIENCY OF ELONGATED PARTICLES

D. Broday, M. Fichman, M. Shapiro* and C. Gutfinger

Faculty of Mechanical Engineering, Technion-Israel Institute of Technology, Haifa 32000, Israel

(*Received* 22 *January* 1996; 15 *April* 1996)

Abstract—The motion of diffusionless elongated spheroidal particles in vertical stagnation flow over a flat collector of a finite size is modelled by calculating hydrodynamic forces and torques acting on a rotating and translating particle. Far above the deposition surface, particle motion is governed by its far upstream initial orientation and geometry. In close vicinity to the surface, where a viscous boundary layer prevails, particles are shown to settle down vertically due to gravity. It is found that the deposition flux of spheroidal particles which are uniformly distributed far above the surface is equal to the flux of spheres with the same settling velocity. On the other hand, randomly oriented spheroids discharged from a point source near the stagnation centerline tend to deposit in the peripheral part of the collector surface. This is in contrast with the comparable behavior of spherical particles, which deposit in a single point on the collector surface.

Effects of the particle geometry, inertial and gravitational forces, initial orientation, and flow parameters on particle deposition are studied by computing particle trajectories. An approximate method is proposed for trajectory calculation, in which particle orientation is frozen and equal to the initial orientation. It is shown that trajectories of the equivalent spheres (having equal volume, or average hydrodynamic resistance, or sedimentation velocity) considerably differ from the true trajectories of spheroidal particles. Significance of the obtained results is discussed in relation to various types of stagnation flows involving aerosol deposition processes and, in particular, to clean room applications. Copyright © 1996 Elsevier Science Ltd

1. INTRODUCTION

In the first paper of this series (Broday *et al.*, 1996, here referred to as Part I) a general model for the motion of particles in vertical stagnation flows was described. These flows are important in various applications, including air sampling, filtration, separation by impactors, and flows in clean rooms. Motion and deposition of micron particles in such flows is a basic behavior with a major significance on technological applications.

In many cases, solid particles generated in industrial production processes have *nonspherical* shapes (Kragelsky *et al.*, 1982). In particular, the length of such nonspherical particles, generated and dispersed during the manufacturing of microchips, can exceed the critical spacing between adjacent conducting lines in microelectronic devices, which is usually taken as one-fifth of the physical spacing (Cooper, 1986). Therefore, deposition of nonspherical contamination particles can result in a bigger damage than that of their equivalent spheres. Deviation of particle shape from spherical (i.e., increasing particle aspect ratio) may enhance their electrostatic deposition (Vincent *et al.*, 1981; Jones *et al.*, 1983). This is attributed to the ability of nonspherical particles to hold larger electrical charges than their equivalent volume spherical counterparts (Vincent, 1985), and to a lower minimal charge needed to significantly augment the deposition rate (Chen and Yu, 1991b). Moreover, it is usually harder to detect by optical instruments nonspherical particles than spheres, since particle thickness (i.e., their minor size) may be comparable to, or less than, the wavelength of the visual part of the spectrum. Thus, malfunctioning of integrated circuits resulting from the deposition of nonspherical particles is more likely to happen (see Gill and Dillenbeck, 1989a, b).

*Author to whom all correspondence should be addressed.

Studies on motion and deposition of nonspherical particles were focused mainly on three flow geometries: (i) internal flows in tubes and channels (Gallily and Eisner, 1979; Asgharian and Yu, 1989; Chen and Yu, 1991a; Podgorski and Gradon, 1990; Shapiro and Goldenberg, 1993; Johnson and Martonen, 1993), (ii) flows over cylinders and spheres relevant to filtration theory (Gallily *et al.*, 1986; Gradon *et al.*, 1989, 1990; Foss *et al.*, 1989), and (iii) flows bounded by a plane wall (Schiby and Gallily, 1980). Recently, Fan and Ahmadi (1995) studied the motion of nonspherical particles in coherent structures prevailing within turbulent flows. No work relevant for the deposition of elongated particles in vertical stagnation flows has been done yet, as far as the authors know.

In Part I we formulated a general model for particle motion in physically realistic vertical stagnation flows. Deposition efficiencies of spherical particles were calculated as quantities independent of the particle initial height above the collector surface. This work deals with the comparable motion and deposition of elongated particles on the basis of that model. We analyze the coupled translational and rotational motions of elongated spheroidal particles in the flow under the influence of gravity. Effects of particle size, shape, initial location and orientation on their trajectories and deposition efficiencies are investigated. The results are discussed in relation to several applications, including particle deposition on horizontal wafers placed on workbenches in laminar-flow clean rooms. The risk of particle deposition on a workbench is evaluated for uniformly distributed contaminant particles in the flow, and for particles discharged from a point source. Other potential applications may include motion of nonspherical particles in cascade impactors (Kasper and Shaw, 1983) and air sampling.

2. PARTICLE EQUATIONS OF MOTION

General equations of motion of a diffusionless nonspherical particle in viscous flow have been described in Part I (see equations (6) and (7) of Part I). Here we use these equations, while specifically referring to axisymmetric prolate spheroidal particles of semi-axes a and l, with the aspect ratio $\beta = l/a > 1$. The particles move in a viscous stagnation flow over a horizontal flat surface of size $2L$ under the influence of gravity (see Fig. 1).

We will mark all dimensional quantities by a tilde " $\sim$ ", thereby reserving the non-marked letters for the following dimensionless quantities:

$$\mathbf{x} = \tilde{\mathbf{x}}/L, \quad t = \tilde{t}U/L, \quad \mathbf{v} = \tilde{\mathbf{v}}/U, \quad \mathbf{u} = \tilde{\mathbf{u}}/U, \quad \boldsymbol{\omega} = \tilde{\boldsymbol{\omega}}L/U,$$

$$\mathbf{K} = \tilde{\mathbf{K}}/a, \quad \mathbf{Q} = \tilde{\mathbf{Q}}/a, \quad \boldsymbol{\Omega}_0 = \tilde{\boldsymbol{\Omega}}_0/a^3, \quad \mathbf{I} = \tilde{\mathbf{I}}/ma^2, \quad \sigma = a/L,$$

$$\mathfrak{R} = \tilde{\mathfrak{R}}L/a^2, \quad \mathrm{D}^2 = \tilde{\mathrm{D}}^2L^2/a^2, \quad \mathrm{Ng} = \frac{mg}{\mu a U}, \quad \mathrm{St} = \frac{mU}{\mu a L}.$$

In the above, $\mathbf{x} = x\mathbf{e}_1 + y\mathbf{e}_2$ denotes the spatial location of the particle center of mass; t is the time variable; $\mathbf{v}$ is the translational velocity of the particle center of mass, expressed in an inertial coordinate frame; $\mathbf{u}$ is the air velocity; $\boldsymbol{\omega}$ is the particle angular velocity; $\mathbf{K}$, $\boldsymbol{\Omega}_0$, and $\mathbf{Q}$ are particle hydrodynamic translational and two rotational resistance tensors, respectively; μ is the dynamic air viscosity; $\mathbf{I}$ is the particle inertia tensor, computed with respect to the particle center of mass which in the present case is also the center of hydrodynamic reaction (Happel and Brenner, 1983); g is the gravitational acceleration; and D^2 and $\mathfrak{R}$ are generalized Laplacian and rotor operators, given by equations (12) and (13) of Part I. These operators, and also $\boldsymbol{\omega}$ and $\mathbf{I}$ are written in the particle-fixed coordinate system. Expressions for the hydrodynamic tensors $\mathbf{K}$, $\boldsymbol{\Omega}_0$, and $\mathbf{Q}$ for spheroidal particles are listed in Appendix of Part I.

In the dimensionless form, the equations of motion are

$$\mathrm{St}\frac{\mathrm{d}\mathbf{v}}{\mathrm{d}t} = \mathbf{A}^{-1}\mathbf{K}\mathbf{A}\left[(\mathbf{u} - \mathbf{v}) + \frac{\sigma^2}{6}\mathrm{D}^2\mathbf{u}\right] - \mathrm{Ng}\,\hat{\mathbf{e}}_2, \tag{1}$$

$$\mathrm{St}\left[\mathbf{I}\frac{\mathrm{d}\boldsymbol{\omega}}{\mathrm{d}t} - (\mathbf{I}\boldsymbol{\omega})\times\boldsymbol{\omega}\right] = \mathbf{Q}(\mathfrak{R}\times\mathbf{u}) - \boldsymbol{\Omega}_0\boldsymbol{\omega}, \tag{2}$$

where **A** is the matrix of the cosines of direction,

$$\mathbf{A} = \begin{bmatrix} \cos\theta & -\sin\theta\sin\phi & \sin\theta\cos\phi \\ \sin\theta & \cos\theta\sin\phi & -\cos\theta\cos\phi \\ 0 & \cos\phi & \sin\phi \end{bmatrix}. \tag{3}$$

Equation (1) of the translational motion is written in an inertial (laboratory) coordinate frame in which the particle translational velocity **v** is measured, and the rotational equation of motion (2) is written in a particle-fixed (noninertial) coordinate system in which the inertia matrix **I** is constant. These coordinate systems are related by the Euler angles via equation (3) (see Fig. 2). Furthermore, particle orientation is related to its angular motion by

$$\tilde{\boldsymbol{\omega}} = -\tilde{\dot{\phi}}\mathbf{e}'_1 + (\tilde{\dot{\psi}} + \tilde{\dot{\theta}}\cos\phi)\mathbf{e}'_2 + \tilde{\dot{\theta}}\sin\phi\mathbf{e}'_3. \tag{4}$$

In contrast with spheres, particle orientation adds additional parameters governing the motion of nonspherical particles over Re (appearing in the normalization of the air

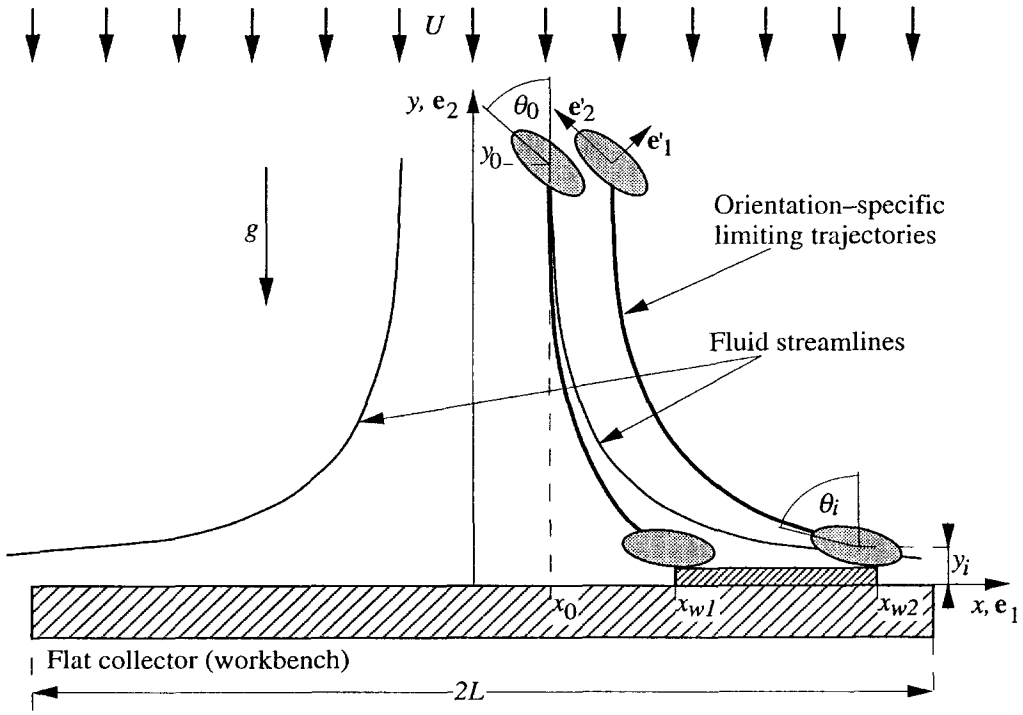

Fig. 1. Schematic of streamlines and particle trajectories in vertical stagnation flow over a flat collector.

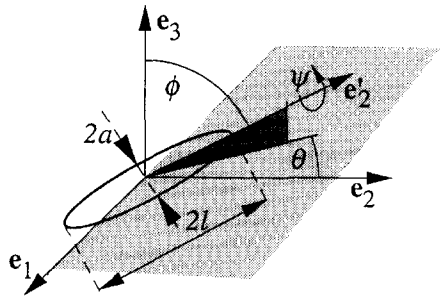

Fig. 2. Euler angles relating the laboratory and the particle-fixed coordinate systems.

velocity field—equation (3) in Part I), σ—the ratio of particle to flow characteristic lengths, the gravitational parameter Ng, and the Stokes parameter St, which is the ratio of the particle relaxation time to the convection time.

The velocity field, appearing in equations (1) and (2), is approximated by a superposition of three two-dimensional basic flows (see Part I):

$$\mathbf{u}(x, y) = \mathbf{u}_v - \mathbf{u}_p + \mathbf{u}_f, \tag{5}$$

where $\mathbf{u}_v$ is the viscous stagnation-point flow, $\mathbf{u}_p$ is the potential stagnation-point flow (both over an infinite plate), and $\mathbf{u}_f$ is the potential flow normal to a plate of finite width of $2L$ (Milne-Thomson, 1968). The above velocity field adequately describes the flow velocity both close to and far from the surface over a wide range of flow Reynolds numbers $\mathrm{Re} = UL/\nu$. In the upstream region the velocity tends asymptotically toward the undisturbed uniform flow where the streamlines are vertical. Close to the surface the flow field approaches the viscous stagnation-point flow (Schlichting, 1987) and accounts for the finite size of the collector plate.

3. DEPOSITION EFFICIENCY

Deposition efficiency, η_t, is a quantity used to characterize the amount of particles deposited between the coordinates x_{w1} and x_{w2} of the collector surface (see Fig. 1). It is defined as the ratio between the actual particle deposition rate, $\dot{n}_A$, and a reference particle stream flowing toward the collector, $\dot{n}_R$, and evaluated far upstream:

$$\eta_t = \frac{\dot{n}_A}{\dot{n}_R}. \tag{6}$$

Consider the case where a spheroidal particle has reached its preferred azimuthal orientation, $\phi = \pi/2$, in a two-dimensional potential (extentional) stagnation flow (Brenner, 1972), but its orientation angle θ continuously changes as a result of rotation induced by flow velocity gradients. In this case, particle orientation is specified by only one angle, θ, varying between 0 and 2π. Consequently, the actual deposition rate, $\dot{n}_A$, appearing in equation (6) may be written as

$$\dot{n}_A = \int_0^{2\pi} \int_{x_{w1}}^{x_{w2}} j_y(x, \theta_i)_{y = y_i(\theta_i)} \, dx \, d\theta_i, \tag{7}$$

where $j_y(x, \theta_i)$ is the orientation-specific vertical component of the particle flux, evaluated at a vertical particle–wall separation $y = y_i(\theta_i)$ which is the interception distance at the moment of capture (Fig. 1). For freely rotating nonspherical particles, this final θ_i-dependent interception distance is not known *a priori*.

The reference particle stream $\dot{n}_R$, appearing in equation (6), is the amount of particles per unit time, crossing at a far upstream location a horizontal surface of area (per unit depth) equal to the projection of $(x_{w2} - x_{w1})$:

$$\dot{n}_R = (x_{w2} - x_{w1}) \int_0^{2\pi} j_{y\infty}(\theta_0) \, d\theta_0, \tag{8}$$

where $j_{y\infty}(\theta_0)$ is the orientation-specific x-independent vertical particle flux in the undisturbed region ($y = y_0$).

For diffusionless particles, the integral in equation (7) may be replaced by a comparable integral at a far upstream location, via the so-called orientation-specific limiting trajectories. These are trajectories of particles which begin to move at a given initial orientation θ_0 and height y_0 from points x_{01}, x_{02}, and end their motion at the points x_{w1}, x_{w2}, respectively, where they touch the wafer surface, $y = y_i(\theta_i)$ (see Fig. 1). Clearly, trajectories of identical particles having identical initial orientations θ_0, but different initial locations x_0, do not intersect. Thus, all identical particles with the same initial orientation θ_0 passing the plane

$y = y_0$ in the interval $x_{01}(\theta_0) < x_0 < x_{02}(\theta_0)$ will deposit on the wafer. Therefore, the integral over θ_i at $y = y_i(\theta_i)$ in equation (7) can be replaced by an appropriate integral over θ_0 at $y = y_0$, namely

$$\dot{n}_A = N\int_0^{2\pi}\int_{x_{01}(\theta_0)}^{x_{02}(\theta_0)} v_y(\theta_0)h(\theta_0)\,dx\,d\theta_0 = N\int_0^{2\pi}[x_{02}(\theta_0) - x_{01}(\theta_0)]v_y(\theta_0)h(\theta_0)\,d\theta_0. \quad (9)$$

In the above equation, we have expressed the particle flux, $j_{y\infty}(\theta_0)$, via the vertical component of the particle orientation-specific velocity $v_y(\theta_0)$, the particle orientation distribution function $h(\theta_0)$, and the particle volumetric number density N, i.e.,

$$j_{y\infty}(\theta_0) = Nh(\theta_0)v_y(\theta_0). \quad (10)$$

Note that the particle-orientation distribution function is assumed to be position-independent in the undisturbed region. It is normalized to yield unity upon integration over all orientations.

The initial coordinates $x_{01}(\theta_0)$ and $x_{02}(\theta_0)$ of the orientation-specific limiting trajectories, appearing in equation (9), ought to be calculated in the course of the solution. Then, integration over θ_0 should be performed for any (e.g., random) orientation distribution function $h(\theta_0)$. The orientation-specific vertical velocity component, v_y, appearing in equation (9) may be determined by (Happel and Brenner, 1983)

$$v_y = -U - \frac{mg}{\mu}\left[\frac{\sin^2\theta_0}{K_{11}} + \frac{\cos^2\theta_0}{K_{22}}\right], \quad (11)$$

where K_{ii} $(i = 1, 2)$ are the components of the translational hydrodynamic resistance tensor. Similarly, the undisturbed particle stream (8) may be expressed as

$$\dot{n}_R = N(x_{w2} - x_{w1})\int_0^{2\pi} v_y(\theta_0)h(\theta_0)\,d\theta_0. \quad (12)$$

In particular, for particles with uniform orientation distribution $h = (2\pi)^{-1}$. Hence, the undisturbed particle flow rate (12) adopts the form

$$\dot{n}_R = N(x_{w2} - x_{w1})\left[-U - \frac{mg}{\mu}\left(\frac{1}{K_{11}} + \frac{1}{K_{22}}\right)\right]. \quad (13)$$

Combining equations (6), (9), and (12), one obtains the total deposition efficiency of spheroidal particles in the form

$$\eta_t(\mathrm{St}, \mathrm{Ng}, \beta, \mathrm{Re}, x_{w1}, x_{w2}) = \frac{\int_0^{2\pi}[x_{02}(\theta_0) - x_{01}(\theta_0)]v_y(\theta_0)h(\theta_0)\,d\theta_0}{(x_{w2} - x_{w1})\int_0^{2\pi} v_y(\theta_0)h(\theta_0)\,d\theta_0}. \quad (14)$$

For spherical particles uniformly dispersed in the undisturbed region, neither of the quantities in equation (14) depends on θ_0. With the use of the velocity field (5), equation (14) yields a y_0-independent deposition efficiency of spherical particles (Part I),

$$\eta_t(\mathrm{St}, \mathrm{Ng}, 1, \mathrm{Re}) = \frac{x_{02} - x_{01}}{x_{w2} - x_{w1}} = \frac{x_0}{x_w}. \quad (15)$$

When all spheroids have the same orientation θ_0^*, the orientation distribution $h(\theta_0)$ can be expressed in the form

$$h(\theta_0) = \delta(\theta_0 - \theta_0^*), \quad (16)$$

where δ is Dirac's delta function. Substitution of equation (16) into equation (14) defines an orientation-specific deposition efficiency, with a functional form similar to the middle term in equation (15),

$$\eta(\theta_0, \mathrm{St}, \mathrm{Ng}, \beta, \mathrm{Re}, x_{w1}, x_{w2}) = \frac{x_{02}(\theta_0) - x_{01}(\theta_0)}{x_{w2} - x_{w1}}, \quad (17)$$

wherein the asterisk is omitted. Numerical simulations, discussed in Section 4, show that the orientation-specific deposition efficiency (17) does not depend either on x_{w1}, x_{w2} (and, hence, on the collector size $x_{w2} - x_{w1}$), or on the initial particle vertical location y_0, i.e.,

$$\eta(\theta_0, \mathrm{St}, \mathrm{Ng}, \beta, \mathrm{Re}, x_{w1}, x_{w2}) = \eta(\theta_0, \mathrm{St}, \mathrm{Ng}, \beta, \mathrm{Re}). \tag{18}$$

Combining equations (14), (17), and (18), one obtains the total deposition efficiency in the form

$$\eta_t(\mathrm{St}, \mathrm{Ng}, \beta, \mathrm{Re}) = \frac{\int_0^{2\pi} \eta(\theta_0, \mathrm{St}, \mathrm{Ng}, \beta, \mathrm{Re}) v_y(\theta_0) h(\theta_0)\, \mathrm{d}\theta_0}{\int_0^{2\pi} v_y(\theta_0) h(\theta_0)\, \mathrm{d}\theta_0}. \tag{19}$$

For particles with a uniform orientation distribution, equation (19) can be simplified by using equation (13) to result in

$$\eta_t(\mathrm{St}, \mathrm{Ng}, \beta, \mathrm{Re}) = \frac{-1}{2\pi}\left[U + \frac{mg}{\mu}\left(\frac{1}{K_{11}} + \frac{1}{K_{22}}\right)\right]^{-1} \int_0^{2\pi} \eta(\theta_0, \mathrm{St}, \mathrm{Ng}, \beta, \mathrm{Re}) v_y(\theta_0)\, \mathrm{d}\theta_0, \tag{20}$$

where v_y is given by equation (11). Note that due to geometrical symmetry of spheroids, the integrals in equations (19) and (20) need to be evaluated in the interval 0–π only.

For the case $\phi = \pi/2$, considered mostly in the present study, only two-dimensional trajectories can be described by the equations of motion (1) and (2). This is due to degeneration of the hydrodynamic translational resistance tensor, written in a laboratory coordinate system, to a symmetrical tensor with only two off-diagonal terms. In a more general case where, in addition to θ_0, particle initial orientation is also specified by the angle ϕ_0, one has $v_y = v_y(\theta_0, \phi_0)$, $h = h(\theta_0, \phi_0)$, and all integrals appearing in equations (7)–(20) are to be replaced by appropriate integrals with respect to these two angular coordinates.

4. SOLUTION METHODS

A nonspherical particle placed in a nonuniform velocity field moves along a certain trajectory while constantly rotating. As discussed in Section 3, calculation of the orientation-specific particle deposition efficiency requires knowledge of the initial locations $x_{0i}(\theta_0)$ ($i = 1, 2$) of the orientation-specific limiting trajectories as data input (see equation (17)). These initial locations can be calculated by a trial-and-error procedure of particle trajectories simulations. These computations account for the coupled translational-rotational motions, and thus constitute a complicated numerical task. One commonly used way to facilitate the calculations is to perform calculations for "equivalent" spherical particles instead of exact integration of equations (1) and (2). These spheres are usually taken either as a volume-equal sphere of the same density, with a radius (Williams and Loyalka, 1991)

$$r_{ev} = a\beta^{1/3}, \tag{21a}$$

or as a mass-equal sphere with the same spatially averaged hydrodynamic resistance $\bar{K}$, with a radius

$$r_{er} = a\frac{\sqrt{\beta^2 - 1}}{\ln(\beta + \sqrt{\beta^2 - 1})}, \tag{21b}$$

or as a mass-equal sphere with the same average sedimentation velocity, with a radius

$$r_{es} = a\sqrt{\frac{\beta \ln(\beta + \sqrt{\beta^2 - 1})}{\sqrt{\beta^2 - 1}}}. \tag{21c}$$

Note that for random orientation distribution of spheroids of revolution, $\bar{K}$ is given by (Happel and Brenner, 1983)

$$\bar{K} = 3\left[\frac{2}{K_{11}} + \frac{1}{K_{22}}\right]^{-1}. \tag{22}$$

In any nonuniform flow field nonspherical particles have preferred orientations. In particular, in stagnation flows (Brenner, 1972) the particle axis of revolution tends to align with the direction of flow extension. We thus perform simulations where the particle moves with several *frozen* orientations, and compare the trajectories of such simulations with the *exact* trajectories, which are calculated using the coupled equations (1) and (2). Deviations between the orientation-frozen and the exact particle trajectories serve to assess the error of the approximate simulations.

In order to solve equations (1) and (2) initial conditions must be supplied, which specify the particle location, orientation, rotational and translational velocities far away from the workbench, where the flow is uniform. At this location, designated by the coordinates (x_0, y_0), we assume that the particles possess their (orientation-dependent) terminal settling velocities, i.e. they move along straight, generally inclined, trajectories (Happel and Brenner, 1983):

$$t = 0: \qquad x = x_0, \quad y = y_0, \quad \theta = \theta_0, \quad \dot{x} = v_{x,t}(\theta_0), \quad \dot{y} = v_{y,t}(\theta_0), \tag{23}$$

where $v_{x,t}$, $v_{y,t}$ are the components of the particle terminal velocity. In particular, $v_{y,t}$ is given by equation (11).

A particle is assumed to be deposited on a smooth surface when it first touches it. That is, particle resuspension and rebound are neglected and simulations terminate at the moment of touching (Fuchs, 1986; Fan and Ahmadi, 1995). The interception distance $y_i(\theta_i)$ depends on the particle geometry and its orientation θ_i prior to capture. The latter is generally not known *a priori*. In orientation-frozen simulations, one deals only with the translational equations of motion (1), with the matrix **A** known from the initial particle orientation. A major benefit of simulating the motion of particles with fixed orientation is that their final orientations and, hence, the interception distances are known. For the general case of rotating-translating particles, a general algorithm for the calculation of the orientation-dependent interception distance at the moment of capture was suggested by Fan and Ahmadi (1995). A much simpler code can be used for particles which move perpendicularly towards the collector surface. This behavior is characteristic of a particle moving in the vicinity of the surface under the influence of gravity (see Section 5), and when particle size is smaller than the boundary layer thickness.

The computations were performed on a Silicon Graphics workstation using the ACSL ver.10 ODE solver. Three different algorithms for numerical integration were checked, namely Gear's stiff variable step and variable order, Adam-Multon's variable step and variable order, and Runga–Kutta–Frehdberg's variable step and fifth order. All the algorithms yielded close results which coincided to within four significant digits.

5. RESULTS

Trajectories of prolate spheroids placed in the given velocity field (5) were computed for various particle aspect ratios, sizes, initial orientations, and initial locations. In addition, calculations were performed for the equivalent spheres of radii r_{ev}, r_{er} and r_{es}, given by equations (21a, b, c), respectively.

Equivalent sphere motion: Figure 3 shows a comparison between trajectories calculated for (i) spheroids performing coupled rotational and translational motion (marked by solid lines), (ii) spheroids with fixed orientations performing translational motion only (marked by circles), and (iii) equivalent spheres. All particles begin their motion from the same location (x_0, y_0) in the undisturbed region. The trajectories of the equal-volume sphere (the dashed line which coincides with the line $\theta_0 = 0$) and of the equal average hydrodynamic resistance sphere (the dotted line) do not adequately represent the trajectories of spheroidal particles due to their lack of sensitivity to particle initial orientation. A similar result (not shown in the figure) has been obtained for the sphere of the same average sedimentation velocity. Thus, modelling of motion of a spheroidal particle as of any of the equivalent

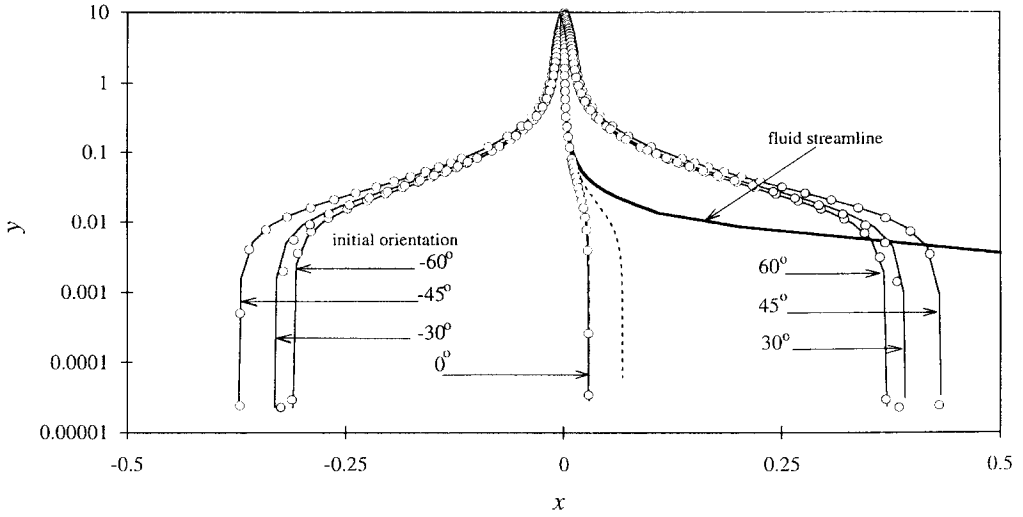

Fig. 3. Trajectories of a spheroidal particle ($\beta = 1.5$) initiating from $x_0 = 0.001$, $y_0 = 10$ with different initial orientations: Re = 6700, Ng = 0.74, St = 0.001. Solid lines—spheroids performing coupled translational-rotational motions, circles—spheroids with fixed orientation, dashed line—equivalent sphere of radius r_{ev} (equation (21a)), dotted line—equivalent sphere of radius r_{er} (equation (21b)).

spheres can lead to large errors. A similar conclusion has also been drawn for other systems, e.g. cyclones (Ingham and Bloor, 1991).

Initial orientation: Trajectories of spheroidal particles are found to be very sensitive to their initial orientations (Fig. 3). Particles moving in the undisturbed region of stagnation flows do not experience an external orienting torque acting upon them and, hence, have no preferred orientation. Particles which begin their motion from about $\theta_0 = \pm 45°$ will deposit farther than those whose initial orientations are close to one of the field principal directions, i.e., 0° and 90° (trajectories of spheroids in the latter orientations are very close, and cannot be distinguished apart in Fig. 3). It may be inferred that the high sensitivity of the trajectories to particle initial orientations implies that the total deposition efficiency (19) should be determined by averaging the orientation-specific deposition efficiency via an appropriate orientation-distribution function $h(\theta_0)$. The latter may be either measured (Bernstein and Shapiro, 1994) or calculated. Below we show that this averaging is unnecessary, and one can utilize previous results obtained for spherical particles in order to calculate the deposition efficiency of elongated particles.

Orientation-fixed trajectories: Figure 3 shows that the trajectories of orientation-fixed particles are very close to the trajectories of freely rotating particles, beginning their motion with the same corresponding initial orientations. The differences between these trajectories (i.e. orientation-fixed and orientation-free) were found to decrease with decreasing aspect ratio. The relative inaccuracy in the determination of particle trajectories stemming from this approximation may amount to 10% for large aspect ratios ($\beta > 100$). However, it is shown below that for the purpose of calculating deposition efficiencies via equations (17)–(19), the difference between two initial x-coordinates $x_{0i}(\theta_0)$, for a given θ_0, can be evaluated sufficiently accurately by the orientation-fixed approximation. This is because the absolute error between trajectories of orientation-fixed and freely rotating particles is small. Nevertheless, all the results discussed below refer to freely rotating particles.

Particle capture: Evolution of particle orientation during its motion is shown in Fig. 4 for different initial orientations, but equal initial location (x_0, y_0). It is seen that, irrespective of the initial orientation, particles terminate their motion almost horizontally, i.e., approach their preferred orientations as discussed in Section 3. Hence, particle final orientation is almost independent of the initial orientation (the latter, however, does affect the deposition

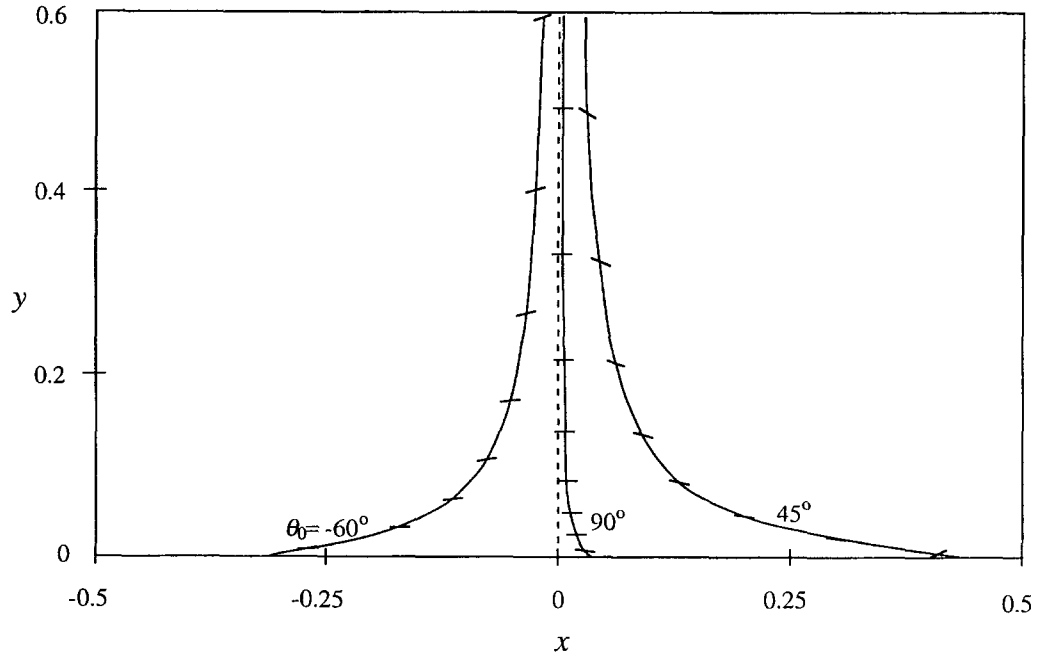

Fig. 4. Orientation evolution for a spheroidal particle ($\beta = 1.5$) moving in a vertical stagnation flow with different initial orientations: $x_0 = 0.001$, $y_0 = 10$, Re = 6700, Ng = 0.74, St = 0.001.

site as shown above). This observation may facilitate the formulation of the particle capture condition, required for termination of the simulations (see Section 4).

In the final part of their trajectories particles move vertically. In typical industrial clean rooms, the Reynolds number based on the workbench width is of the order of 5000–10,000. For these values of Re, the flow is characterized by a hydrodynamic boundary layer prevailing adjacent to the workbench surface. For the above Re, the thickness of this layer is of order $\sim 0.03L$, where L is the half-width of the workbench. Furthermore, the above described vertical segments of the trajectories span over a distance of order $0.003L$. That is, the vertical segments in the particle trajectories prior to capture expand no more than 10% of the thickness of hydrodynamic boundary layer. Hence, capture of micrometer particles occurs as a result of settling due to the gravity force rather than interception. Generalizing that result, this implies that interception, as a capture mechanism, is irrelevant for particle deposition in stagnation flows when $\sigma\beta\sqrt{\mathrm{Re}} < 0.1$. This, in turn, facilitates the condition for termination of the numerical calculations, as discussed in Section 4. It follows that the exact and orientation-frozen trajectories differ also in particle interception distance at the moment of capture. This difference, however, has a weak effect on the deposition site since the final trajectory segments are normally short. The above observation, however, may not be valid in other applications, as well as for very slender particles whose lengths may exceed the final vertical segments of the particle trajectories. In addition, when inertial effects prevail, particles may obtain orientations which are different from those discussed above, especially in the vicinity of the symmetry line. In particular, this has been described in impactors by Kasper and Show (1983) (see also a discussion in Section 6).

Particle trajectories: Trajectories of spherical particles in vertical stagnation flows have the following property (see Part I):

$$\frac{x_{01}}{x_{w1}} = \frac{x_{02}}{x_{w2}}, \tag{24}$$

which allows definition of a universal trajectory. For nonspherical particles, universal trajectories in the above form do not exist even for particles starting their motion with identical orientations. This is because even in the case of settling in an undisturbed flow, the

trajectories of obliquely oriented nonspherical particles are not parallel to the direction of gravity. Rather, particles drift horizontally when neither of the particle principal directions coincides with the principal directions of the body-force field (Happel and Brenner, 1983). Moreover, due to this horizontal drift, nonspherical (e.g. spheroidal) particles may cross the field symmetry line and deposit on the opposite half of the surface (see Figs 3 and 4). For a given range of initial orientations, a spheroidal particle beginning its motion far enough from the surface (i.e., at large y_0) may cross the field symmetry plane for any x_0.

Figure 5 depicts trajectories of spheroidal particles of St < 0.01 and the same aspect ratio, $\beta = 27$, but of different Ng. It is seen that as particle settling velocity increases, i.e., Ng grows, deposition occurs closer to the symmetry axis. This is similar to the behavior observed for spherical particles (see Part I).

Figure 6 depicts the effect of aspect ratio, β, on particle trajectories. One can see that for a given Ng, spheroidal particles with larger aspect ratios shift horizontally much further than particles with lower β. With β decreasing to 1, the trajectory approaches that of a sphere of equal mass and having the same average sedimentation velocity, with the radius r_{es} given in equation (21c).

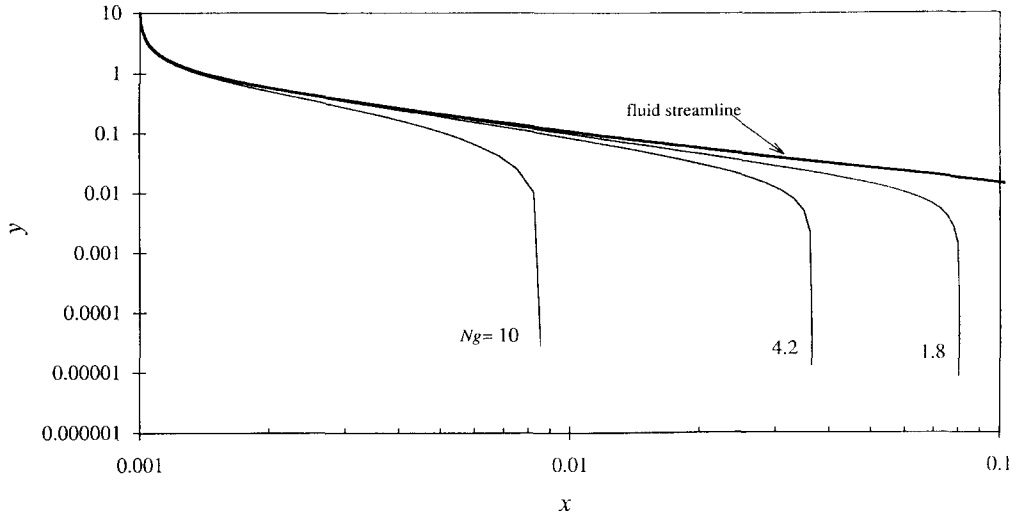

Fig. 5. The effect of Ng on trajectories of spheroidal particles: $x_0 = 0.001$, $y_0 = 10$, $\theta_0 = 90°$, Re = 6700, $\beta = 27$.

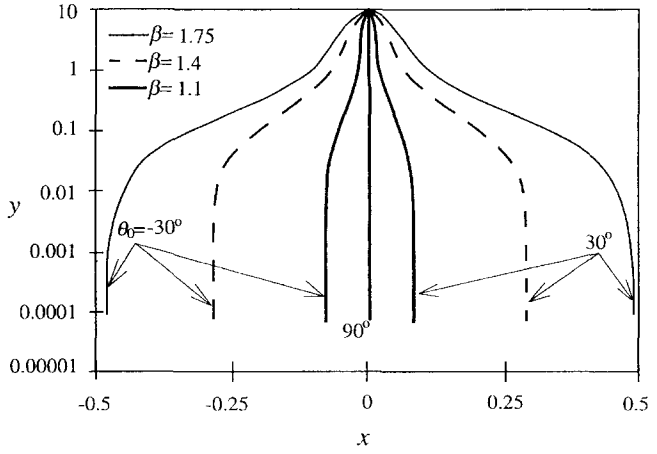

Fig. 6. The effect of particle aspect ratio on its trajectories for various initial orientations: $x_0 = 0.001$, $y_0 = 10$, Re = 6700, Ng = 5, St = 0.1.

Normally, the thickness a of elongated particles, such as polymeric chains, and fibers made of asbestos, glass, wool, linen, or cotton, varies much less than their length l (Cheng, 1986; Asgharian and Yu, 1989). Trajectories of spheroidal particles of the same minor radius a but different lengths l are shown in Fig. 7. As expected, trajectories of heavier particles, characterized by larger β, are steeper, causing the particles to deposit closer to the symmetry axis for all initial orientations.

Deposition site: The influence of the initial orientation on the deposition site, x_f, is summarized in Fig. 8, where one can see a strong dependence of x_f on β. Particles of any aspect ratio travel along the farthest trajectory above the collector surface if their initial orientation is $\theta_0 = \pm 45°$. This is unlike the case of spheroids settling in a stagnant fluid, where the maximal trajectory inclination angle (with respect to the gravity direction) depends on β (Happel and Brenner, 1983). Moreover, for the given parameters (Ng = 0.1, $x_0 = 0.001$), as the aspect ratio increases beyond about 2.5, particles with certain initial orientations never deposit on the collector. For $\beta > 5$, particles beginning their motion with almost all initial orientations do not deposit on the collector at all. From all slender

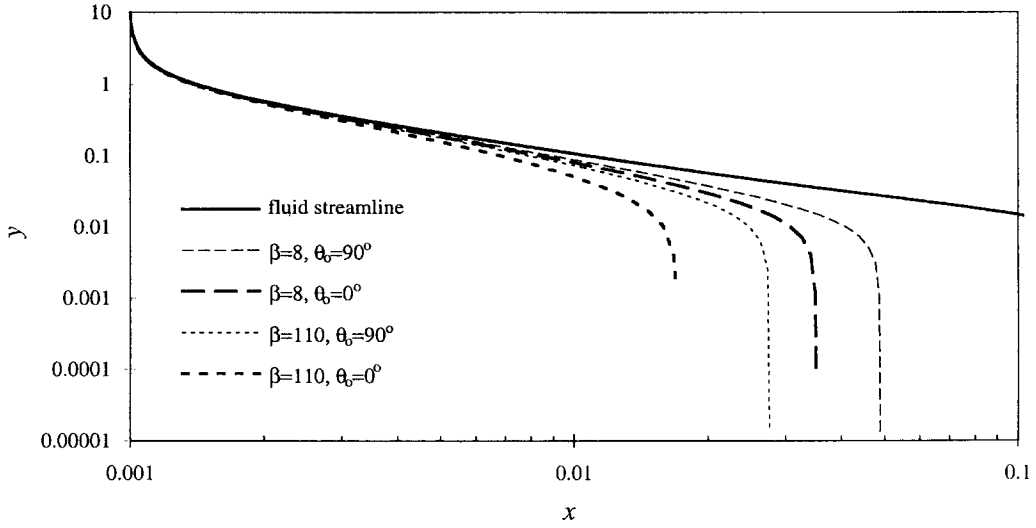

Fig. 7. The effect of particle length on its trajectories: $x_0 = 0.001$, $y_0 = 10$, Re = 6700, $a = 4.5$ μm.

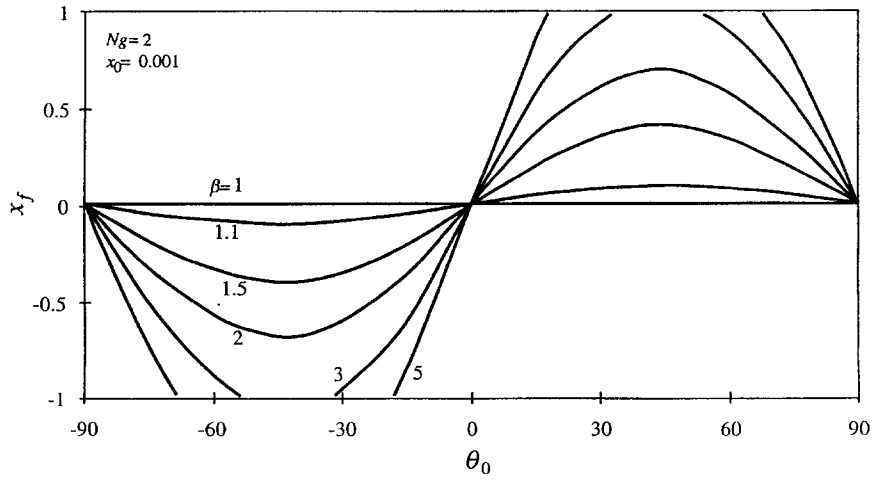

Fig. 8. Variation of particle deposition site with respect to its initial orientation: $x_0 = 0.001$, $y_0 = 10$, Re = 6700, Ng = 2, St = 0.05.

spheroidal particles moving down toward the collector, only those are captured whose initial orientation angle θ_0 is close to 0^0 or 90°, which are the principal directions of the body-force field. Hence, a randomly oriented oblong spheroidal particle coming from a given location (e.g., $x_0 = 0.001$) has less opportunities to deposit on the collector than any of its equivalent spheres.

Effect of the initial location x_0: The above results mean that from all similar elongated particles located initially at x_0, it may happen that only a small portion, possessing certain initial orientations θ_0, will deposit on a wafer placed on a workbench between the coordinates x_{w1} and x_{w2} (Fig. 8). Thus, it may be inferred that the deposition efficiency of elongated particles is always less than that of the sphere with equal Ng. This is, however, not true, since the above calculations (Fig. 8) pertain to particles beginning their motion only at $x_0 = 0.001$. It turns out that identical particles originating from different initial locations and having certain appropriate initial orientation angles $\theta_0 = \theta_0(x_0)$ will deposit on the same wafer. To show this, consider Fig. 9 exhibiting the effect of x_0 on the deposition site. It is seen that the effect of changing x_0 is to shift the particle deposition site x_f by a value which is independent of β. Indeed, the curve $x_f(\theta_0, x_0)$ may be obtained by shifting the comparable curve calculated for any other x_0 by a value Δx_f dependent on Δx_0, but independent of θ_0 and β. This conclusion may also be drawn from the constant slope of the inclined lines in Fig. 10, plotted for $\theta_0 = 45^\circ$. The distance Δx_f may thus be calculated for the equivalent sphere of the same settling velocity Ng as the spheroid.

Figure 10 depicts the deposition site x_f vs the initial location x_0. The curves are straight lines with the same (β-independent) slope. For *spheres*, characterized by a deposition efficiency $\eta_s = \eta_s(\mathrm{Ng})$, x_f is (see Part I)

$$x_f = \frac{x_0}{\eta_s(\mathrm{Ng})}. \tag{25}$$

In contrast to equation (25), Figs 9 and 10 indicate that for *spheroidal* particles, x_f has the following functional form:

$$x_f = \frac{x_0}{\eta_s(\mathrm{Ng})} + F(\beta)\sin(2\theta_0). \tag{26}$$

The coefficient F is assumed to be independent of particle orientation, and to be liable only on particle aspect ratio. Figure 11 depicts the function $F(\beta)$ defined in equation (26). It is

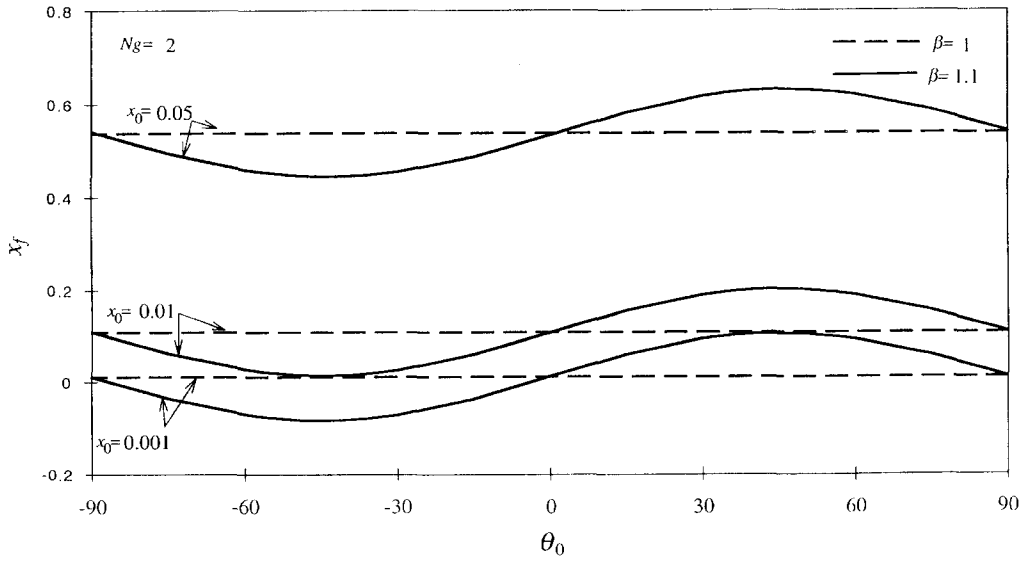

Fig. 9. The effect of x_0 on the deposition site x_f: $y_0 = 10$, Re = 6700, Ng = 2, St = 0.05.

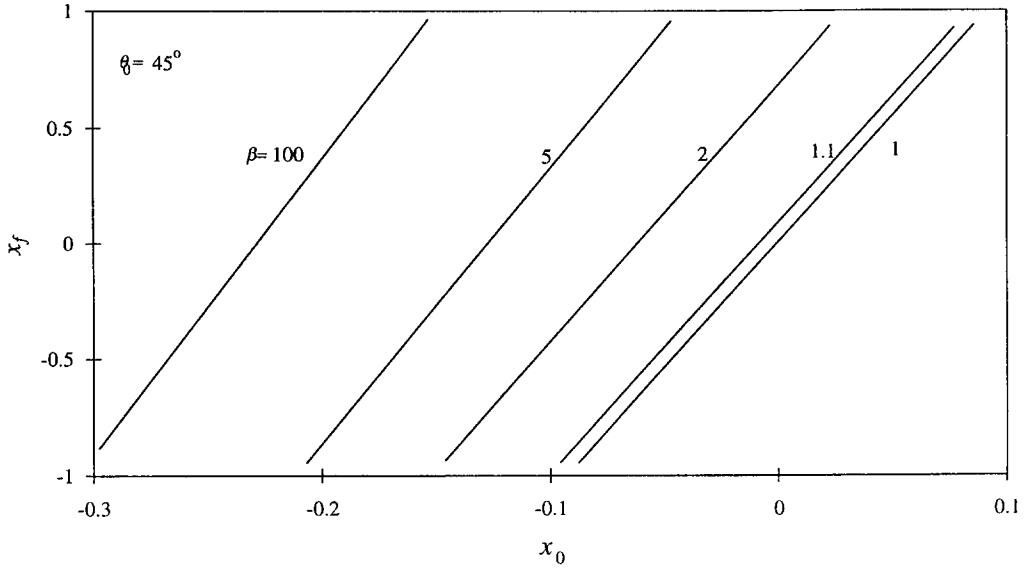

Fig. 10. The relation between particle deposition site and its initial location for various particle aspect ratios: $y_0 = 10$, $\theta_0 = 45°$, Re = 6700, Ng = 2, St = 0.05.

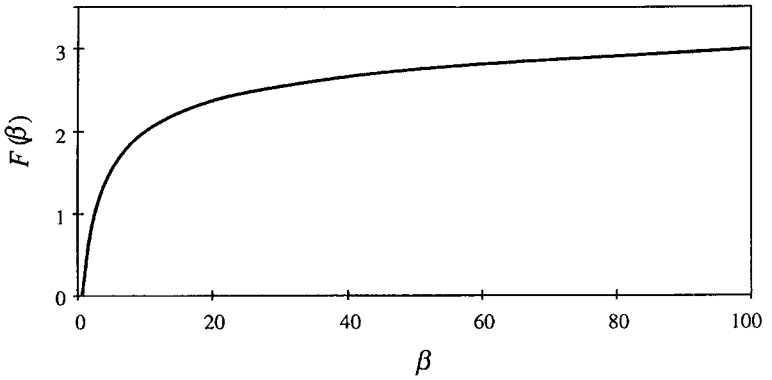

Fig. 11. The function $F(\beta)$ defined in equation (26). The plot coincides for Ng = 0.6, 0.1, and 5.6. The expression given in equation (27) matches this line with no observable differences.

seen to be independent of the particle settling velocity Ng. A least-square approximation of $F(\beta)$ with a relative error not exceeding 2% is

$$F(\beta) \cong 1.76 \ln[\ln(\beta) + 1][1 - 1.07 \exp(-\sqrt{\beta})]. \tag{27}$$

The total deposition efficiency η_t (equation (19)) can now be calculated by substituting x_f from equation (26) in place of x_w in equation (17). This procedure shows that η_t of spheroidal particles is equal to η_s of spherical particles of the same Ng. The latter is given in Part I. This observation is true for a wide range of β when deposition is unaffected by the interception (which is the case when $\sigma\beta\sqrt{\mathrm{Re}} < 0.1$), and as long as the orientation distribution is random at y_0.

Deposition from a point source: Figure 12 depicts the distribution of particles (of a given Ng and β) deposited along the workbench, which are discharged from a point source (i.e., a jet) at $x_0 = 0$ with a uniform orientation distribution. Although such particles may deposit in a relatively wide x-domain, a sharp peak of the deposition density is observed, which is shifted to the peripheral part of the workbench with increasing β. Particles from a wide orientation interval (30–60°) deposit within 1% area around the maximal deposition site. Deposition from an air stream uniformly loaded with particles may be considered as

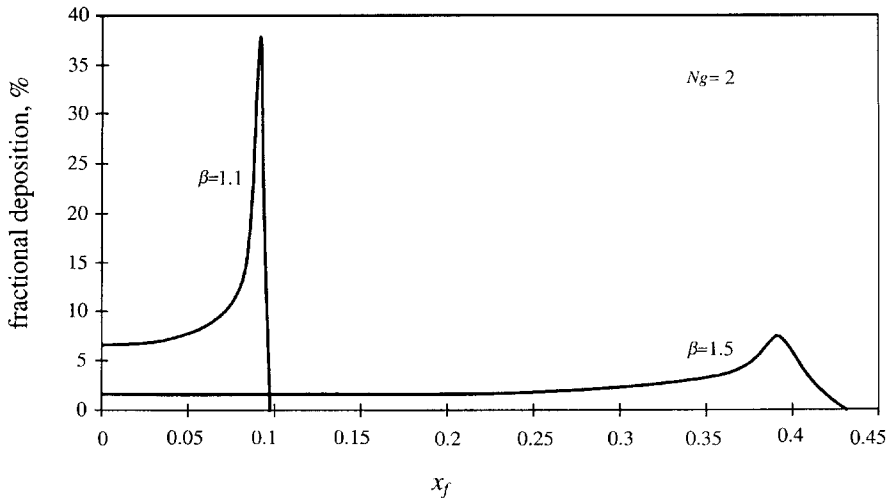

Fig. 12. The spatial distribution of deposited particles originating with random orientations from a point source at $x_0 = 0$, $y_0 = 10$: Ng = 2, St = 0.05, Re = 6700.

a continuous superposition of point sources at different locations x_0 in an otherwise clean air. Each of these sources yields a distribution similar to the one shown in Fig. 12, however, shifted by a distance proportional to x_0. When these shifted plots cover the whole collector surface, a uniform deposition pattern prevails, with particle deposition efficiency given by equation (19).

Equation (19) is generally valid for infinitely extended uniform particle distribution. In practice, however, it might be used also for jet-like aerosol streams of finite width, provided that (for given x_{w1}, x_{w2}) all the values of $x_{01}(\theta_0)$, $x_{02}(\theta_0)$ from which deposition is possible (equation (17)) lie within the bounds of the jet source. This case is usually called wide stream deposition (Fuchs, 1986). However, sufficiently narrow jets do not cover the entire range of $x_{01}(\theta_0)$, $x_{02}(\theta_0)$ from which particles may deposit on a given wafer. For such aerosol jets the deposition rate of randomly oriented oblong particles will be lower than that of spheres of the same Ng, and hence their deposition efficiency cannot be calculated as for spheres. This conclusion is especially true for jets containing particles of nonuniform orientation distribution (see also the discussion in Section 6).

Consider a horizontal region far upstream, from which particles can potentially deposit on the workbench. This means that at any given point of this region, one can always find at least one orientation which leads to particle deposition on the workbench. Clearly, this region is symmetric with respect to the centerline, and hence can be characterized by width $\Delta^* x_0$. This quantity can be evaluated by considering trajectories of the particles with initial orientations $\theta_0 = \pm 45^\circ$, since such particles reach deposition sites which are farthest from their initial locations (Figs 3 and 8). Inserting $\theta_0 = \pm 45^\circ$ and $x_f = \mp 1$ in equation (26), one obtains the following expression for $\Delta^* x_0$:

$$\Delta^* x_0 = 2\,\mathrm{Ng}[1 + F(\beta)]. \tag{28}$$

Clearly $\Delta^* x_0$ increases with increasing particle aspect ratio since, for a given a, both Ng and $F(\beta)$ increases with l. Therefore, limiting ourselves by a maximal expected particle length, say l_{max}, $\Delta^* x_0(l_{max})$ represents the size of the region from where all particles with $l < l_{max}$ can arrive and deposit on the collector (e.g., the whole workbench). Thus, in order to prevent contamination, one should largely be concerned with regions from which potential contamination particles may come. As such, equation (28) may be used for risk assessment for deposition of nonspherical contaminant particles in clean rooms.

6. DISCUSSION

For simplicity, we have chosen in most of the simulations $\phi_0 = \pi/2$. In that case θ_0 is the only angle which determines particle orientation and trajectory. However, several simulations were also performed with $\phi_0 \neq \pi/2$. These simulations show that trajectories of spheroidal particles in the flow field (5) are mainly affected by the angle between the gravity direction and the major particle axis, $(\widehat{\mathbf{e}_2, \mathbf{e}'_2})$. This is due to a relatively weak dependence of the hydrodynamic drag force components on particle orientation. That is, the ratio between the lateral component and the longitudinal component of the drag force acting on a spheroid reaches a maximal value of 2 when $\beta \to \infty$. In contrast to the minor effect that the orientation exerts on the hydrodynamic forces, particle orientation with respect to the direction of gravity has a dramatic effect on the trajectory. Simulations performed for gravity-free particles reveal that for all practical means, particle trajectories are almost independent of the initial orientation. Thus, it is preferable to define particle orientation with respect to the direction of gravity (or another dominant body force) rather than with respect to the characteristic flow direction.

The viscous particle–wall interactions were shown to be significant in a close vicinity to the wall surface $\tilde{y} < 10l$ (Hsu and Ganatos, 1989). Beyond this region, one can evaluate the viscous forces and torques as in the undisturbed flow with an error not exceeding 5%. Yet, the hydrodynamic force acting on settling spheroidal particles towards a flat wall hardly depends on the particle–wall separation (Hsu and Ganatos, 1989). The wall effect was found to diminish with increasing particle aspect ratio β (Gavze and Shapiro, 1996). For $\sigma\beta\sqrt{\mathrm{Re}} < 0.1$, as in the present study, the distance $10l$ is much smaller than the thickness of the hydrodynamic boundary layer (in the cases studied less than 10% of it), which implies that the velocities are low. Hence, in this region the trajectories of particles moving towards a horizontal surface in a gravity field are almost vertical, and particle orientations are almost constant.

To estimate the hydrodynamic wall effect, we note that inertialess spheroidal particles moving near a solid wall (where the flow is close to simple shear flow) acquire vertical lift and horizontal drift velocities (Gavze and Shapiro, 1996). In the hydrodynamic boundary layer, the drift velocity may be estimated (in a dimensionless form) as

$$v_{x,\mathrm{d}} = kx\sigma\beta\sqrt{\mathrm{Re}}, \tag{29}$$

with the coefficient k of order unity. For a small ratio $\sigma = a/L$, this velocity is small and barely affects particle trajectories. The wall-induced lift velocity is even smaller than the drift velocity (Gavze and Shapiro, 1996). In view of the above estimates, one may conclude that, due to small values of the parameter $\sigma\beta\sqrt{\mathrm{Re}} < 0.1$, the wall effect is negligible as compared with the influence of gravity.

Particle hydrodynamic interactions, as computed in the present study, are based on the creeping flow assumption, i.e., $\mathrm{Re}_\mathrm{p} \ll 1$. For small particles ($\sigma \ll 1$) moving in close proximity to the surface, where the flow may be approximated by a simple shear, the above condition yields that

$$l^2(\partial u_x/\partial y)/\nu \ll 1, \tag{30}$$

where u_x is the x-component of the air velocity and l the particle length. Expressing the shear rate by using the numerical results obtained for viscous stagnation flow (Schlichting, 1987), one obtains

$$x(\sigma\beta)^2\,\mathrm{Re}^{3/2} \ll 0.813. \tag{31}$$

This may serve as a criterion for the validity of the creeping flow assumption. This criterion is usually satisfied for clean room conditions where $\mathrm{Re} \approx 5000$–$10{,}000$ and $\sigma \approx O(10^{-5})$. Furthermore, equations (30) and (31) can serve as criteria for the validity of the creeping flow assumption to other types of stagnation flows, in particular for flows over cylindrical and spherical collectors (in filtration-related applications) and in impactors. For such

applications one can identify $2L$ with the collector diameter D, and use in equation (30) the pertinent expression for the velocity gradient (e.g., from known analytical solutions for viscous flows around bodies of various shapes).

The velocity field used in the present study is composed of three basic two-dimensional flows, two of them are potential flows. Any potential (i.e., irrotational) flow satisfies the Stokes flow equations. Thus, the use of potential flow components $\mathbf{u}_p$ and $\mathbf{u}_f$ (see equation (5)) in the generalized Faxen law (equations (10) and (11) in Part I) is legitimate. On the other hand, the viscous term $\mathbf{u}_v$ constitutes an exact solution of the Navier–Stokes equations, obtained with nonnegligible inertia terms. For such flows, the derivation of the generalized Faxen law (Happel and Brenner, 1983) is not valid, since they are applicable for flows in which the inertia terms are omitted. Therefore, strictly speaking, a linear combination of the three flows (5) cannot be used for the calculation of particle hydrodynamic interactions by means of the generalized Faxen law. To support our approach we note that the generalized Faxen expressions for the hydrodynamic force and torque are exact for uniform and shear flows. Any arbitrary flow field, which may be inertial at a certain (large) length scale (say L), may be viewed as a creeping flow at a sufficiently small scale—comparable to the particle size l. Moreover, use of the Faxen law for drag calculations of small (Brownian) particles is also justified by the Stokes–Einstein relation (based on the convective–diffusion transport equation) which is commonly employed for all flows (Bird *et al.*, 1960).

The finite-size flat collector surface (i.e. workbench geometry), as employed in this work, is characterized by sharp edges at $x = \pm 1$. Accordingly, the flow field used here has singularities at these points, in the vicinity of which the velocity grows to infinity due to not accounting for separation of the flow from the surface (Lesnic *et al.*, 1994). This may have an influence on the particle deposition flux upstream (i.e., at smaller x). However, for a domain (wafer) located sufficiently far from the edges, the deposition efficiency is not affected by the edge effects. In addition, edge effects diminish with decreasing distance between the particle and the workbench surface (Dagan *et al.*, 1982). More elaborate computer calculations of flow fields over realistic flat collectors geometries, which are free of sharp edges, or accounting for separation of the flow at the plate edges, can provide a better evaluation of the particle deposition flux in the plate margin regions.

It was found in Section 5 that when $\mathrm{St} < 0.01$ and $\sigma\beta\sqrt{\mathrm{Re}} < 0.1$, the deposition efficiency of spheroidal particles uniformly distributed in the undisturbed flow is equal to that of spheres with the same dimensionless settling velocity Ng. This is because nonspherical particles coming from different locations x_0 tend to deposit on the collector as a result of their orientation-dependent horizontal drift. In contrast to this so-called wide stream deposition (Fuchs, 1986), a different situation occurs when these particles come from a jet, as in cascade impactors. In this case the range of possible locations x_0 is quite narrow, so many particles miss the collector plate. Thus, nonspherical particles with a uniform orientation distribution and originating from jet sources will deposit in smaller amounts than their spherical counterparts.

In reality, elongated particles tend to align themselves with the flow streamlines, as has been shown experimentally by Kasper and Shaw (1983) for the deposition of long-chain aggregates in impactors. Generally, particle motion in these devices is controlled by inertia forces. However, particles which arrive at the peripheral part of the flow (far from the jet center) move in the air for a sufficiently long time, exceeding their characteristic relaxation time $m/\mu a$. These particles behave like inertialess, i.e., they align themselves with the flow streamlines (as in Fig. 4). On the contrary, elongated particles moving close to the jet center tend to orient themselves vertically till the moment of impaction. As a result, the orientation of particles deposited in this central region is random (Kasper and Shaw, 1983), which clearly results from the inertial effects governing their motion. In addition, there might be a significant effect of chain (initial) orientation in the jet that affects its motion, especially near the centerline (cf. Fig. 3). This may have a spreading effect on the deposition site and on the total amount of particles deposited on each impactor stage, which might explain partially some of the results found by Kasper and Shaw (1983) for the wide size distributions (in terms of the aerodynamic diameter) of deposited chains.

The efficiency calculations performed here assume perfect particle capture with no bouncing. In fact, the probability of particle sticking to a solid surface depends on several factors, including inertia, angle of impaction, properties of the surface, etc. (Wang, 1986). Generally speaking, the finer the particles, the lower the impaction velocity, and the closer the impaction angle to $\pi/2$, the greater the sticking probability. Moreover, elongated particles are more likely to stick to surfaces than spheres of the same volume (Fuchs, 1986). This process, however, should be further investigated.

7. CONCLUSIONS

We showed that trajectories of individual spheroidal particles may be approximated reasonably well by calculating only the translational motion of the particles, with their initial orientation fixed. However, the error, resulting from this approximation, in computing particle trajectories increases with β. Trajectories of all equivalent spheres (i.e., of the same settling velocity, volume, aerodynamic drag, etc.) differ significantly from those of the spheroidal particles because they do not take into account the orientation-dependent particle horizontal drift in a gravity field. In particular, a spheroidal particle can cross the flow symmetry plane and deposit on the opposite half of the collector surface.

The deposition efficiency of a swarm of noninteracting spheroidal particles in vertical stagnation flows is the same as that of the equivalent spherical particles with the same settling velocity, Ng. This observation holds for particles uniformly dispersed far above the collector surface, and as long as the interception capture mechanism does not affect the deposition, that is $\sigma\beta\sqrt{\mathrm{Re}} < 0.1$. This is true in spite of the significant influence of particle shape and orientation on each individual trajectory: even a small deviation from sphericity results in considerable effects on the deposition site of a given particle. Therefore, the decision whether to look at a particle as a sphere or as a fiber depends on the specific goals of the investigation.

Deposition sites of spheroidal particles can be calculated from equations (26) and (27) via the deposition efficiency of spherical particles (Part I). A simple expression (28) is proposed for the size of the far upstream region from which particles may deposit on the collector. The size of this region is proportional to Ng and increases with the particle aspect ratio.

The deposition distribution of nonspherical particles discharged from a point source with random initial orientations has a distinguished peak, resembling qualitatively the expected deterministic deposition pattern of elongated particles discharged from an aerosol jet with orientations close to the preferred orientation. For aerosol streams with uniform orientation distribution, the location of this peak in the deposition distribution is shifted to the peripheral part of the collector plate when particle aspect ratio increases.

Acknowledgement—This research was supported in part by The Israel Ministry of Science and Arts.

REFERENCES

Asgharian, B. and Yu, C. P. (1989) A simplified model of interceptional deposition of fibers at airway bifurcation. *Aerosol Sci. Technol.* **11,** 80–88.

Bernstein, O. and Shapiro, M. (1994) Direct determination of the orientation distribution function of cylindrical particles immersed in laminar and turbulent shear flows. *J. Aerosol Sci.* **25,** 113–136.

Bird, R. B., Stewart, W. E. and Lightfoot, E. N. (1960) *Transport Phenomena.* Wiley, New York.

Brenner, H. (1972) Dynamics of neutrally buoyant particles in low Reynolds number flows. *Prog. Heat Mass Transfer* **6,** 509–574.

Broday, D., Fichman, M., Shapiro, M. and Gutfinger, C. (1996) Motion of diffusionless particles in vertical stagnation flows. Part I—general theory and deposition efficiency of spheres. *J. Aerosol Sci.* **28,** 23–34.

Chen, Y. K. and Yu, C. P. (1991a) Sedimentation of fibers from laminar flows in a horizontal circular duct. *Aerosol Sci. Technol.* **14,** 343–347.

Chen, Y. K. and Yu, C. P. (1991b) Sedimentation of charged fibers from a circular duct flow. *J. Aerosol Sci.* **22,** 747–756.

Cheng, Y. S. (1986) Bivariate lognormal distribution for characterizing asbestos fiber aerosols. *Aerosol Sci. Technol.* **5,** 359–368.

Cooper, D. W. (1986) Particulate contamination and microelectronics manufacturing: an introduction. *Aerosol Sci. Technol.* **5,** 287–299.

Dagan, Z., Pfeffer, R. and Weinbaum, S. (1982) Axisymmetric stagnation flow of a spherical particle near a finite planar surface at zero Reynolds number. *J. Fluid Mech.* **122,** 273–294.

Fan, F. G. and Ahmadi, G. (1995) A sublayer model for wall deposition of ellipsoidal particles in turbulent streams. *J. Aerosol Sci.* **26,** 813–840.

Foss, J. M., Frey, M. F., Schamberger, M. R., Peters, J. E. and Leong, K. M. (1989) Collection of uncharged prolate spherical aerosol particles by spherical collectors I—2-D motion. *J. Aerosol Sci.* **20,** 515–532.

Fuchs, N. A. (1986) Methods for determining aerosol concentration. *Aerosol Sci. Technol.* **5,** 123–143.

Gallily, I. and Eisner, A. (1979) On the orderly nature of the motion of nonspherical aerosol particles I—deposition from a laminar flow. *J. Colloid Interface Sci.* **68,** 320–337.

Gallily, I., Schiby, D., Cohen, A. H., Hollander, W., Schless, D. and Stober, W. (1986) On the inertial separation of nonspherical aerosol particles from laminar flows I—the cylindrical case. *Aerosol Sci. Technol.* **5,** 267–286.

Gavze, E. and Shapiro, M. (1996) Particles in a shear flow near a solid wall: effect of non-sphericity on forces and velocities. *Int. J. Multiphase Flow* (accepted).

Gill, P. and Dillenbeck, K. (1989a) Using snake patterns to monitor defects and enhance VLSI device yields. *Microcontamination*, February, p. 23.

Gill, P. and Dillenbeck, K. (1989b) Using snake patterns to monitor defects and enhance VLSI device yields. *Microcontamination*, March, p. 33.

Gradon, L. and Podgorski, A. (1990) Flexible fibrous particle behavior in the carrier gas flow around cylindrical obstacle. *Chem. Engng Sci.* **45,** 3435–3441.

Gradon, L., Podgorski, A. and Grzybowski, P. (1989) Deposition of flexible and stiff fibrous particles. *J. Aerosol Sci.* **20,** 971–974.

Happel, J. and Brenner, H. (1983) *Low Reynolds Number Hydrodynamics*. Martinus Nijhoff, The Hague.

Hsu, R. and Ganatos, P. (1989) The motion of a rigid body in viscous fluid bounded by a plane wall. *J. Fluid Mech.* **207,** 29–72.

Ingham, D. B. and Bloor, M. I. G. (1991) The efficiency of the cyclone for irregularly shaped particles. *Aerosols—Their Generation, Behavior, and Applications, Proc. 5th Ann. Conf. and Particle Shape Workshop*, pp. 235–240.

Johnson, D. L. and Martonen, T. B. (1993) Fiber deposition along airway wall: effect of fiber cross-section on rotational interception. *J. Aerosol Sci.* **24,** 525–536.

Jones, A. D., Johnston, A. W. and Vincent, J. H. (1983) In *Aerosols in the Mining and Industrial Work Environments* (Edited by Marple, V. A. and Liu, B. Y. H.), pp. 613–632. Ann Arbor Science, Ann Arbor, MI.

Kragelsky, I. V., Dobychin, M. N. and Kombalov, V. S. (1982) *Friction and Wear Calculation Methods*. Pergamon Press, Oxford.

Lesnic, D., Elliott, L. and Ingham, D. B. (1994) The influence of separation on the collection efficiencies of obstacles. *J. Aerosol Sci.* **25,** 527–533.

Milne-Thomson, L. M. (1968) *Theoretical Hydrodynamics*, 5th Edition. MacMillan, London.

Podgorski, A. and Gradon, L. (1990) Motion and deposition of flexible particles in laminar gas flow through a pipe. *J. Aerosol Sci.* **21,** 957–967.

Schiby, D. and Gallily, I. (1980) On the orderly nature of the motion of nonspherical aerosol particles III—the effect of particle-wall fluid dynamic interaction. *J. Colloid Interface Sci.* **77,** 328–352.

Schlichting, H. (1987) *Boundary Layer Theory*, 7th Edition. McGraw-Hill, New York.

Shapiro, M. and Goldenberg, M. (1993) Deposition of glass fiber particles from turbulent air flow in a pipe. *J. Aerosol Sci.* **24,** 65–87.

Vincent, J. H. (1985) *J. Aerosol Sci.* **16,** 511–519.

Vincent, J. H., Johnston, W. B., Jones, A. D. and Johnston, A. M. (1981) *Am. Ind. Hyg. Ass. J.* **42,** 711–721.

Wang, H. C. (1986) Theoretical adhesion efficiency for particles impacting a cylinder at high Reynolds number. *J. Aerosol Sci.* **17,** 827–837.

Williams, M. M. R. and Loyalka, S. K. (1991) *Aerosol Science, Theory and Practice, with Special Applications to the Nuclear Industry*. Pergamon Press, Oxford.